Journal of Hydrology 502 (2013) 68–76

Contents lists available at ScienceDirect

Journal of Hydrology

journal homepage: www.elsevier.com/locate/jhydrol

Can electrical conductivity data from a single pumping test provide information about the location of a neighboring mixing zone between two aquifers? An example from Aix-les-Bains/Marlioz (Savoie, France)

Jean-Yves Josnin[a,*], Stephanie Gallino[b], Philippe Renard[c]

[a] Laboratoire EDYTEM, Université de Savoie/CNRS, Pôle Montagne, Campus Scientifique, F-73376 Le Bourget-du- Lac, France
[b] Independent Hydrogeologist (Freelance), 20 Route du Revard, F-73100 Mouxy, France
[c] Centre d'Hydrogéologie et de Géothermie de Neuchâtel (CHYN), Rue Emile Argand 11, CH-2000 Neuchâtel, Switzerland

ARTICLE INFO

Article history:
Received 5 March 2013
Received in revised form 19 July 2013
Accepted 22 July 2013
Available online 17 August 2013
This manuscript was handled by Corrado Corradini, Editor-in-Chief, with the assistance of Fritz Stauffer, Associate Editor

Keywords:
Electrical conductivity
Single well test
Mixing thermal and shallow waters
Alps

SUMMARY

Pumping tests were first developed to interpret observed drawdown in wells. Analyses of drawdown and temperature profiles now help petroleum geologists and geothermal-energy specialists improve production rates, and numerous hydrogeological studies have combined drawdown data with measures of electrical conductivity or a chemical parameter (often a pollutant). The present study used electrical conductivity data from a pumping test in a single well to obtain information about the position of the hydrothermal plume that feeds Aix-les-Bains' Thermes de Marlioz spa. Applying this data to a 3D model of an equivalent porous medium showed that the plume at the bottom of the subsurface aquifer must be downstream from the well. In the present study, combining drawdown data for a single well with electrical-conductivity measurements provided an efficient method for determining the position of a mixing zone near pumped wells. This method may well be generalizable to other situations.

1. Introduction

Pumping tests were first developed to interpret observed drawdown in a piezometer or single well, with the aim of determining an aquifer's transmissivity and storage coefficient, or, in some cases, the distance to the boundaries where an aquifer mixes with another aquifer or a river. The earliest methods could only be applied to homogenous aquifers (Theis, 1935; Cooper and Jacob, 1946; Boulton, 1954; Hantush, 1956), but researchers have developed increasingly sophisticated approaches that can now be applied to even the most heterogeneous cases (Warren and Root, 1963; Hamm and Bidaux, 1996; Jourde et al., 2002; Lods and Gouze, 2004; Riva et al., 2009). Nevertheless, pumping tests often lead to non-unique interpretations (Leven and Dietrich, 2006) and are still based on descriptions of a homogenous medium to which several heterogeneities have to be added (Renard, 2005a,b).

The earliest method was derived by Theis (1935) from a procedure that had previously been used to resolve thermal problems. Today, petroleum geologists and geothermal-energy specialists regularly use simultaneous monitoring of drawdown and temperature to obtain information about hydrodynamic parameters and thereby devise ways of increasing oil or heat production (see, for example, Boberg, 1966; Keys and Brown, 1978; Miller, 1979; Grant et al., 1983; Woodbury and Smith, 1988; Sagar et al., 1991; Bataillé et al., 2006).

Numerous studies have combined measures of electrical conductivity or a chemical parameter (often a pollutant) with drawdown data, generally applying one of two approaches. In the first approach, a chemical tracer test is combined with data from a pumping test (Vandebohede and Lebbe, 2006), in which case pumping test interpretations are combined with numerical modeling in order to determine the dispersivity of the medium (essentially the longitudinal dispersivity, α_L). The second approach uses integral pumping tests to characterize the dispersivity of the medium (in the present case, the transverse dispersivity, α_T) by observing the behavior of a pollution plume that is traversed by a line of observation piezometers (e.g., Bauer et al., 2004; Kalbus et al., 2007).

In the present study we investigated the mixing of a hydrothermal plume with a superficial aquifer by combining the results of a pumping test in a single well with measurements of drawdown, temperature and electrical conductivity. Our aim was to determine

* Corresponding author. Tel.: +33 4 79 75 87 43; fax: +33 4 79 75 81 71.
E-mail addresses: Jean-Yves.Josnin@univ-savoie.fr (J.-Y. Josnin), stephaniegallino@yahoo.fr (S. Gallino), Philippe.Renard@unine.ch (P. Renard).

0022-1694/$ - see front matter © 2013 Elsevier B.V. All rights reserved.
http://dx.doi.org/10.1016/j.jhydrol.2013.07.029

the position of the hydrothermal plume that supplies Aix-les-Bains' Thermes de Marlioz spa.

Mixing between a hydrothermal plume and a subsurface aquifer is a common phenomenon in the northern French Alps, occurring in numerous localities, including Aix-les-Bains, La Léchère, Saint-Gervais-les-Bains, Salins-les-Thermes, and Brides-les-Bains. (cf. Siméon, 1980; Vuataz, 1982; Gallino, 2007; Thiébaud et al., 2010; Sonney, 2010). However, the only studies to have been carried out in most localities are hydrogeochemical investigations of spa outlets (springs, boreholes) to determine the percentage of mixing between two aquifers.

2. Geographical and geological settings

Aix-les-Bains is located on the western edge of the northern French Alps, 60 km south of Geneva (Fig. 1). Three spa establishments within a few kilometers of Aix-les-Bains currently exploit the area's underground water resources. The Thermes de Marlioz spa, just south of the city center, uses hypothermal water; the Thermes Nationaux, in the city center, uses hyperthermal waters; and the Société des Eaux d'Aix-les-Bains bottles mineral water at Raphy Saint Simon, just north of the city.

Aix-les-Bains lies within the southern end of the molasse basin that extends from Chambéry in France to Linz in Austria. The area is bordered to the west by the southern tip of the Jura Mountains and to the east by the western edge of the sub-Alpine Bauges Mountains. Geologically, the area is characterized by an alternating series of limestones and marls. The most massive limestones form both the structural folds and the karst aquifers, whereas the marl horizons form extensive impervious layers. In general, the fold train runs N–S and is overfolded to the west. Anticlines (Montagne de la Charvaz, Mont du Corsuet) have been thrust over synclines (Lake Bourget syncline) by a succession of faults injected with evaporites (Gallino et al., 2010). To the north, the Chambotte anticline is a lower amplitude and higher altitude structure (see Mont du Corsuet in Fig. 1b for its southern tip). The eastern flank of the fold is truncated by two backthrust faults. To the south, the Roche du Roi anticline is broader and lower in altitude. A peel thrust that has been injected along the overlap thrust (Fig. 2b) disappears toward the south and is not present at the Thermes de Marlioz (Fig. 2a).

The recharge zone of the thermal system is in the Upper Tithonian to Valanginian limestones of the Montagne de la Charvaz, on the west side of Lake Bourget (Fig. 2). This is the only catchment in the study area where precipitation greatly exceeds aquifer discharge and runoff. Due to the overlying Hauterivian marls and the synclinal structure of Lake Bourget, the recharged waters percolate to a depth of 2200 m. They then follow the fault plane along which the Aix-les-Bains anticlinal dome has been thrust over the Lake Bourget syncline, becoming mineralized with Cl, SO_4, Na and K ions. Below Aix-les-Bains, the mineralized waters enter a series of vertical fractures that crosscut all the beds of the Aix-les-Bains anticlinal dome (from Upper Tithonian to Barremian). The hydrothermal plume waters rise through these fractures at the bottom of the Barremian limestones (Fig. 2). Hydrothermal flows mix with the superficial east-to-west flowing aquifer in the Barremian strata on the western flank of the upper part of the anticline (Gallino, 2007). Recharge in these Barremian strata occurs in zones where the marls and thin sandstones of the Chattian–Aquitanian series are absent or are very thin (as shown in Fig. 2).

The two following paragraphs are more precise both about the local geology and about the local hydrogeology around the Thermes de Marlioz spa.

The Thermes de Marlioz spa is at the southern end of the known hydrothermal upwelling. As noted above, the peel thrust that oc-

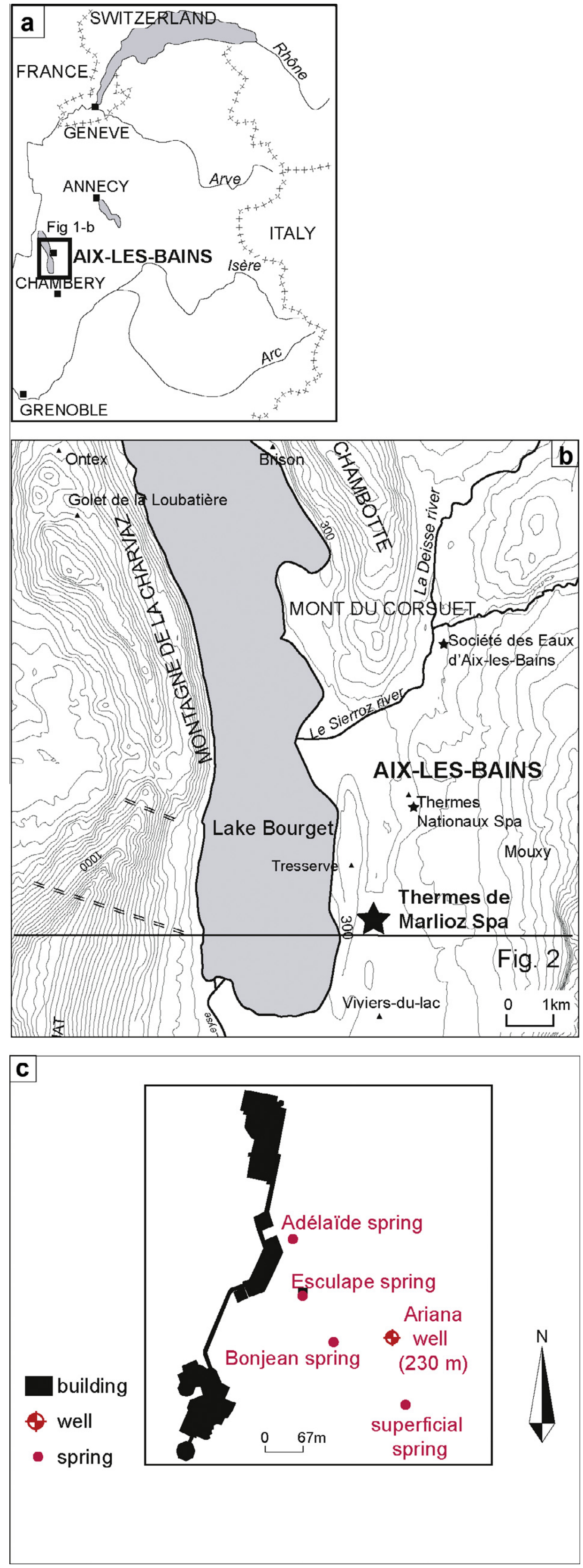

Fig. 1. Location of the study area (a) within the region, (b) the Aix-les-Bains area, and (c) the Aix Marlioz area.

curs to the north (Fig. 2b) is absent in the cross-section shown in Fig. 2a. Nevertheless, all the other geological structures in the top part of the anticline are present from north to south. There is no

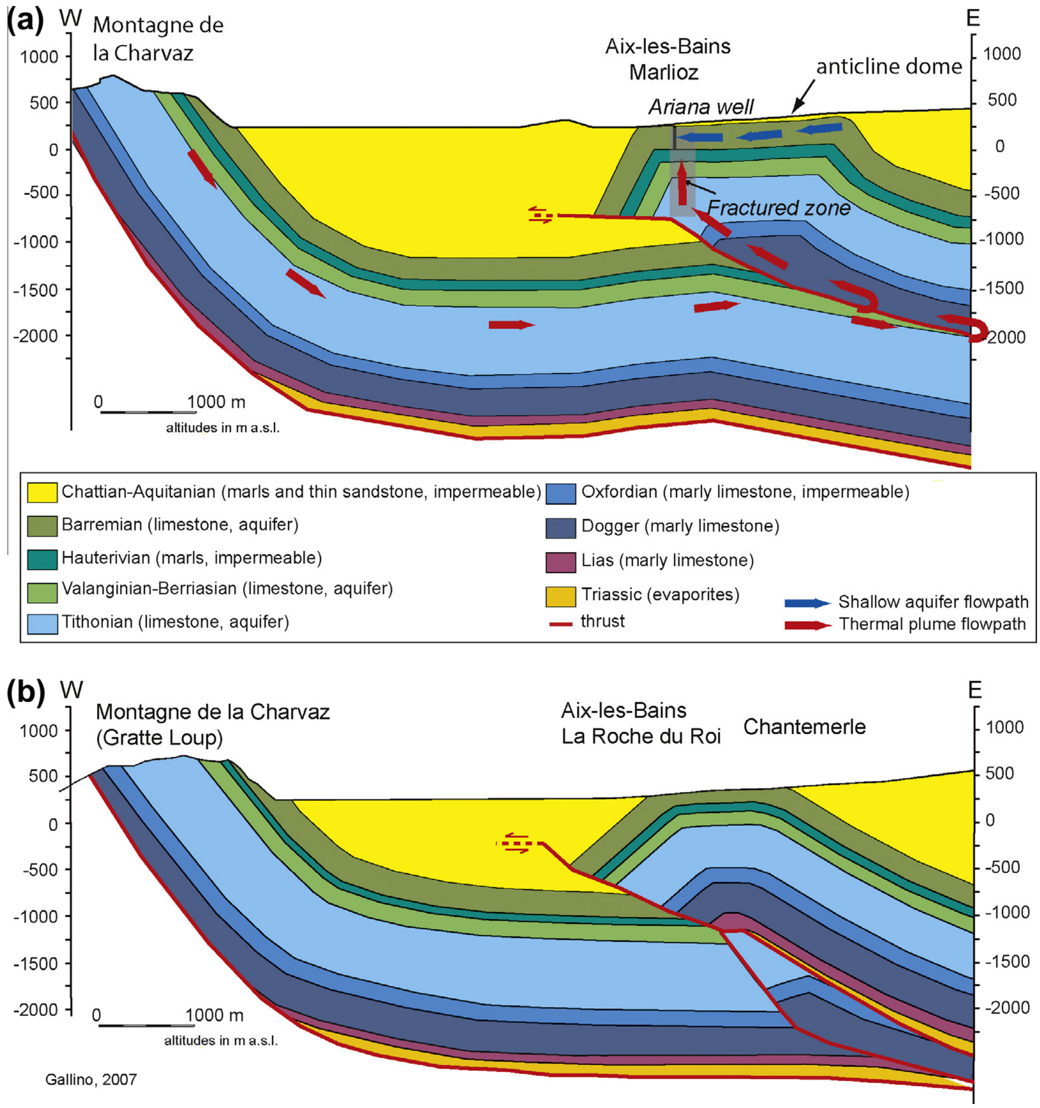

Fig. 2. East–west geological cross-section of the Aix-les-Bains overlapping anticline from the South at Aix Marlioz (a), that is the studied area, to the North at the Roche du Roi (b).

evidence of karstification, either at outcrop or in the Ariana well (in contrast to the Thermes Nationaux spa); the Ariana well log merely shows a very permeable zone (fractured zone or cataclastic zone). Due to the absence of karstification, the flow rates of the natural outlets (Adelaïde, Bonjean and Esculape springs, locations shown in Fig. 1c) range from 0.5 to 15 L min^{-1} and discharge temperatures range from 13 to 17 °C (these values are around 20 L s^{-1} and 40 °C at the Thermes Nationaux spa, where karstification is observable at outcrop).

In terms of chemical composition, the Thermes de Marlioz waters are bicarbonate calcic to sodic waters (Fig. 3). Of all the Thermes de Marlioz springs, the Adelaïde spring has the most similar chemical composition to the thermal plume. The Bonjean and Esculape springs, and the Ariana well, have mixed chemical compositions, with lower total dissolved solids (TDS). In particular, the sulfate and sodium contents of these outlets are significantly lower, because these ions are not present in the shallow aquifer. The fact that the Thermes de Marlioz springs temporarily dried up during the drilling of the Ariana well is further evidence of interaction between the Thermes de Marlioz outlets. A comparison of the chemical compositions of the Adelaïde spring and the two

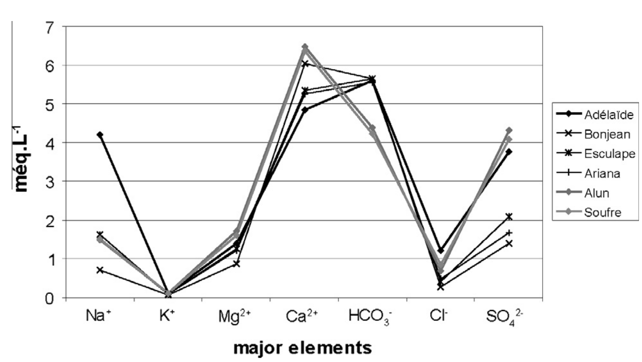

Fig. 3. Major element concentrations for the four Aix Marlioz outlets, in black, and comparison with the two Thermes Nationaux natural outlets, in grey. The Adelaïde spring, in bold black, is the least mixed (or nonmixed) outlet at Aix Marlioz. The characteristics of the other three Aix Marlioz outlets (which are all similar) suggest mixing between the Adelaïde water and the bicarbonate calcic water of the shallow aquifer. A comparison between the Adelaïde and Thermes Nationaux springs reveals differences in their HCO3− and Na+ contents, indicating that the upwelling zones are distinct.

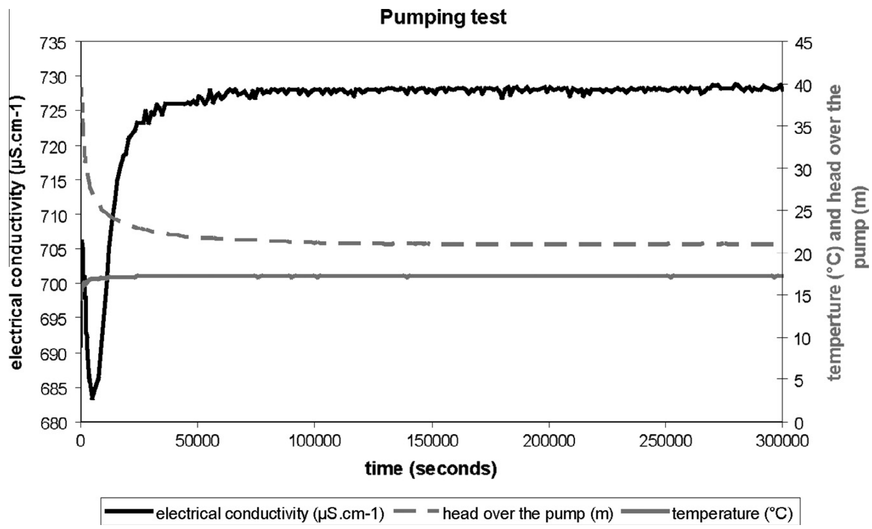

Fig. 4. Graph showing drawdown, electrical conductivity and temperature measurements taken during the real pumping test on the Ariana well at Aix Marlioz.

Thermes Nationaux (Alun and Soufre) springs (Fig. 3) shows that the upwelling plume at the Thermes de Marlioz spa is more carbonated and sodic. Thus, the upwelling at the Thermes de Marlioz spa must come from the general aquifer system described by Gallino et al. (2009), but it follows a different terminal pathway that emerges in a non-karstic setting, at the bottom of the Barremian carbonate series.

3. Data acquisition

Our study of mixing in the aquifer was based on a pumping test carried out on the Ariana well (Figs. 1 and 2). The well is cased to a depth of 180 m, below which it continues as a borehole to a depth of 230 m, where it enters the impermeable Hauterivian marls, in which it stops. It has a diameter of 0.15 m and has been drilled into an unconfined zone. During the test, we measured drawdown, temperature and electrical conductivity (Fig. 4).

The temperature curve (Fig. 4) showed an extremely slow but regular increase in temperature, in marked contrast to the electrical conductivity curve, which showed large oscillations at the start of pumping. Our initial analyses showed that these oscillations on the electrical conductivity curve could not have been caused by a measurement probe malfunction or a well-bore storage effect. Then, if the probe or a well-bore storage effect is not the cause, we conclude that the shape of the electrical conductivity curve is the consequence of the distribution of flows into the aquifer around the well. We used a 3D model to examine configurations that could produce this type of hydrodynamic behavior.

4. Modeling

We built a three-dimensional model using the Feflow groundwater finite-element simulator (Diersch, 1996), which can be used to carry out running simulations that encompass both mass transport and thermal parameters (thermohaline simultaneous mass and heat transport). We assumed a linear relationship between the electrical conductivity and total mineralization of the water, which allowed us to use solute transport in the model to take into account electrical conductivity variations (in the model, the solute was taken to represent the water's total mineralization (TDS)). In the modeled aquifer, the extreme values of TDS range from 600 to 1050 mg L^{-1}, as shown in Fig. 5b, that corresponds to a 0.25‰ variation of the fluid density according to the Stuyfzand formula as used in Holzbecher (1998). In the model, the temperature ranges from 11 °C (surface) to 19 °C (temperature of the plume at the aquifer bottom), which lead this time to a 1.15‰ variation of the fluid density (always from Holzbecher, 1998). We then considered that the temperature and electrical conductivity differences between the two mixed waters and the very local emergence of the plume would not allow convective cells to form. Consequently, we used the divergence forms of the transport equations for mass transfer:

$$\frac{\partial}{\partial t}(\phi RC)+\frac{\partial}{\partial x_i}(q_i^f C)-\frac{\partial}{\partial x_i}\left(D_{ij}\frac{\partial C}{\partial x_j}\right)+\phi R\lambda C=Q_C \qquad (1)$$

and for heat transfer:

$$\frac{\partial}{\partial t}[(\phi\rho^f c^f+(1-\phi)\rho^5 C^5)T]+\frac{\partial}{\partial x_i}(\rho^f q_i^f c^f T)-\frac{\partial}{\partial x_i}\left(\Lambda_{ij}\frac{\partial T}{\partial x_j}\right)=Q_T \qquad (2)$$

In the above equations, C is the concentration, φ is the porosity, D_{ij} is the dispersive-diffusive tensor, R is the retardation factor, λ is the decay rate, $\rho^f c^f$ and $\rho^s c^s$ are the volumetric heat capacities of the fluid and of the solid, respectively, T is the temperature, t is the time, Λ_{ij} is the heat transfer tensor, q is the Darcy velocity, and Q_C and Q_T are the mass flow and heat flow, respectively. Although the temperature values and the TDS values ranges lead to negligible density variations, the minimal Feflow parameterization takes into account the density dependencies from a unique factor that defines the influence of thermal expansion on fluid density (linear dependency), but the fluid viscosity dependencies are neglected. Gravity acts along the negative y-axis direction.

4.1. Mesh

Assuming that the geometry of the geological structures does not change from north to south (see above), we used a vertical mesh along a west–east cross-section and extended it horizontally north–south (Fig. 5). This mesh takes into account the area's topography and the dip of the strata on the western flank of the anticline. It is refined around the well and the fractured/more permeable zones in the Barremian limestones, so that the strong hydraulic gradients in this sector did not generate calculation errors. The final model had 517,080 elements composed of 6 nodded triangular prisms.

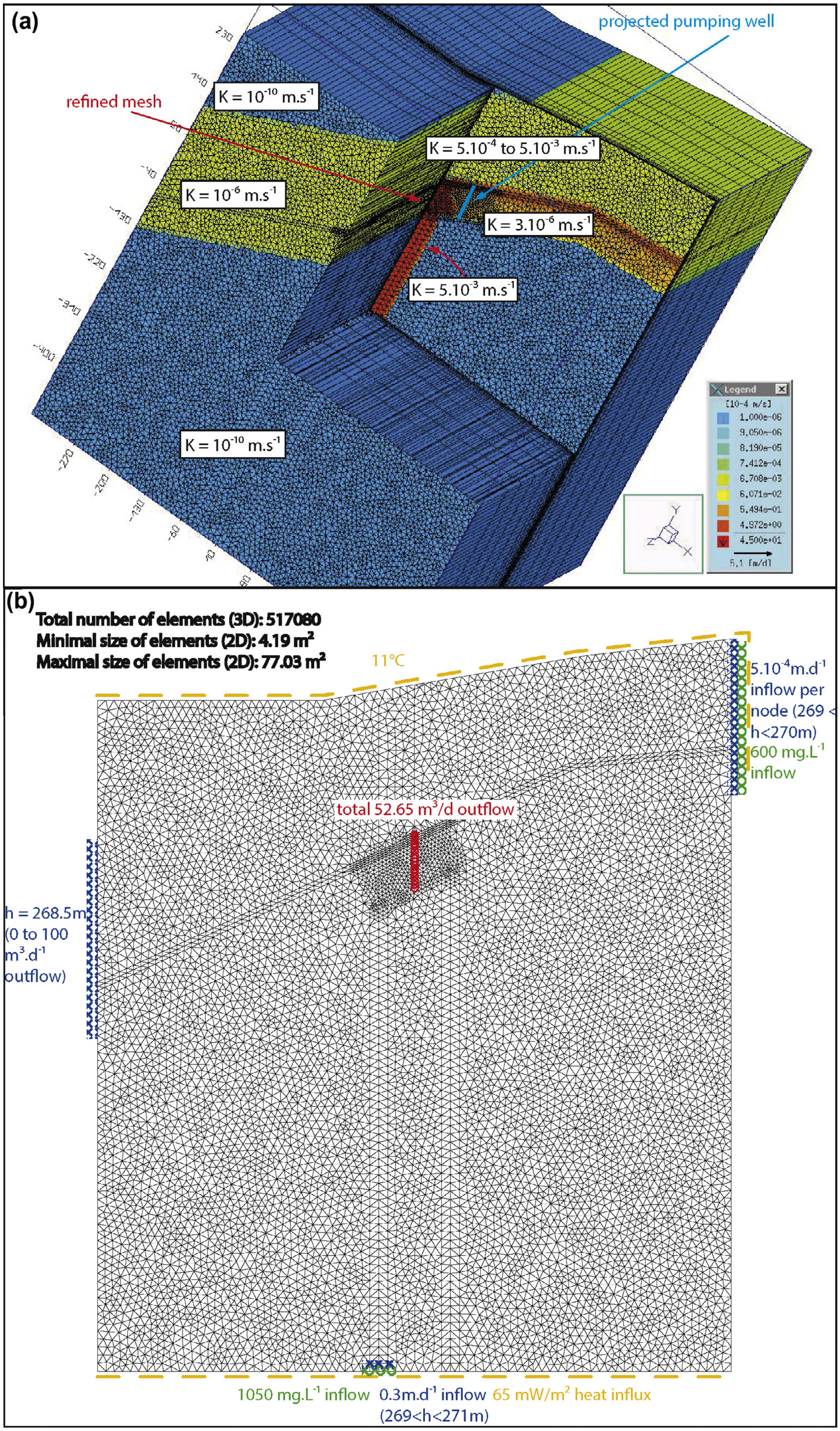

Fig. 5. 3D finite-element model of the area around the Ariana well at Aix Marlioz, for the case of a thermal plume located downstream from the pumping well. (a) 3D view where color-coding is used to show hydraulic conductivities. Main values of hydraulic conductivities are indicated in addition to the 3D projection. Dispersivities are homogenous. Gravity acts along the negative *y*-axis. Model dimensions are in m. (b) 2D view of a layer including the plume upwelling. The well is projected on this slice. The flow boundary conditions types are shown in blue and the constraints indicated into brackets. The mass transport boundary conditions are shown in green. The heat transport boundary conditions are shown in orange. The pumping well is projected in red. The minimal and maximal size of the elements in the cross section is indicated in m^2.

The quality of the mesh was estimated by calculating the percentage of triangles with obtuse angles and the percentage of triangles that did not comply with the Delaunay criterion (i.e. the circumcircle of a triangle must not contain the apex of another triangle). In the case of the Aix-Marlioz model, these triangles accounted for only 2.5 and 0.7% of all triangles, respectively, which is acceptable. In the area containing the strongest hydraulic gradients, the minimum and the maximum distance between nodal points in the three dimensions are 0.5 m and 14 m respectively.

The modeled zone represents an 800 m $\times$ 800 m $\times$ 800 m section of the aquifer. This size permits to have none or only a negligible effect along the boundaries of the model both on the pressure state and on the transport (the mean pumping rate is around 6.1×10^{-4} m^3 s^{-1} during the simulation time). It allows reasonable CPU time. Finally, the modeled zone is small enough to be out of the influence zone of the Northern plume of the Thermes Nationaux spa.

4.2. Boundary conditions

The boundary conditions are summarized in Fig. 5b.

For the flow we applied a 0.3 m d^{-1} inflow at the bottom of the upwelling zone, constraining the head within a range that is consistent with the existence of natural outlets. We applied another head-condition constrained inflow (of 5×10^{-4} m d^{-1} per node) to the upstream side of the shallow aquifer, and a constant head condition to the downstream side of the shallow aquifer (Lake Bourget lies downstream from the model and acts as the regional base level). We did not add any inflow from the surface because the pumping test was performed during a dry period.

In terms of transport, we used two Neumann-type conditions as the boundary conditions. The first condition, applied to the input flow on the upstream side of the shallow aquifer, was considered to be representative of the total mineralization at this location. Indeed, a spring without any mineralization characteristic of the thermal plume is present on the studied zone (superficial spring in Fig. 1c) with a total mineralization of 600 mg L^{-1}. The second condition, applied to the bottom of the upwelling, was the plume's mineralization, estimated to 1050 mg L^{-1} considering that the TDS value of Adelaïde spring is quite inferior to the TDS value of the plume.

In terms of heat flow, we used air temperature as the temperature for the surface of the model topography and applied the local geothermal flux to the bottom of the model. As for the model described in Gallino et al., 2009, a geothermal flux of 65 mW/m^2 was specified at the bottom of the model (Lucazeau and Vasseur 1988). This value is the mean of the fluxes measured in two oil exploration boreholes drilled by Esso Rep (1976) north of Aix-les-Bains.

4.3. Calibration

In order to calibrate the model's hydraulic conductivities, we used a similar range of hydraulic conductivities to that used for the general model described in Gallino et al., 2009. The hydraulic conductivities values are shown in Fig. 5a. Because only the flow in the shallow aquifer interested us, we did not make any details under the Hauterivian marls that are the shallow aquifer bottom (i.e. the series under the Hauterivian marls were modeled as impermeable). Although some 2D elements can be introduced into the Feflow mesh, we did not try to exactly reproduce the fractures in the aquifer in our initial simulations. For this preliminary study we limited ourselves to an equivalent, more-or-less heterogeneous porous medium, taking into account known and postulated fracturing. We allowed for the more "fractured" zone at the top of the borehole (layer showing cataclasis, cf. above) by adding a very permeable zone parallel to the stratification in the corresponding part of the model. We added another very permeable zone along the upwelling plume pathway (Fig. 5a).

The range of dispersivities (between zero and several meters) was consistent with the size of the modeled area (800 m $\times$ 800 m $\times$ 800 m) and with commonly used values for the major ions (e.g., for NaCl see Bester et al., 2006). The results shown in Fig. 6 were obtained with a longitudinal dispersivity α_L = 5 m and a transversal dispersivity α_T = 0.5 m. These are the default values proposed by Feflow but tests suggested that they are reasonable values for the present case.

The heat capacity and thermal conductivity of the rocks and the water were uniform throughout the mesh. The FEFLOW default heat capacity value (2.52×10^6 J/m^3/K) was used for the solid phase, as the literature indicates values of around 2.43×10^6 J/m^3/K for limestones and 2.52×10^6 J/m^3/K for dolomites (Waples and Waples, 2004). As several authors (Özkahraman et al., 2004; Pfingsten et al., 2001) have reported mean solid thermal conductivity values of 2 W/m/K for limestones, this value was used in the present study. FEFLOW default values were used for the thermal conductivity (0.65 W/m/K) and heat capacity (4.2×10^6 J/m^3/K) of water.

The robustness of the model was also tested by increasing the number of elements in order to ensure that charges were not simulated using erroneous calculations resulting from insufficiently fine meshing.

The Peclet and Courant numbers obtained during the simulations were less than 1 and 2, respectively, because the time steps and the mesh were of limited size, and the maximal effective velocities obtained were below 10^{-4} m s^{-1}. This explains the low Peclet and Courant numbers obtained for the whole simulation. These values are consistent with those recommended by Perrochet and Bérod (1993).

During the simulations, the automatic time step control via predictor-corrector schemes was applied.

The initial conditions corresponded to the functioning of the Ariana well with the current boundary conditions during 10 years (Ariana well supplies the Thermes de Marlioz spa). The "equilibrium" obtained in head, mass and heat transfer was then broken during 2 days by stopping the pumping. The simulation began at this moment, when the data registration starts and the pump functioned again.

5. Results and discussion

5.1. Position of the heterogeneities

With respect to transport modeling, we focused only on the shapes of the curves and did not try to exactly reproduce the measured values. This explains why, in Fig. 6, the range of amplitude variations in the best matches for the shape of the curves is around 15 µs cm^{-1}, whereas the measured values were 50 µs cm^{-1} (Fig. 4). This was also the case for the simulation times. Our aim was not to obtain a perfect calibration, but to show that for a certain set of parameters the answer given by the hydrodynamic flow and mass transport is coherent with the data and provides information about the position of the heterogeneities.

Following a first trial-and-error calibration, several shapes remained possible, especially for the electrical conductivity graphs, depending on the position of the hydrothermal plume with respect to the well.

The hydrodynamic and chemical data available for the springs (see Fig. 1b for their location and Fig. 3 for major element concentrations) indicate that the well is not directly above the thermal plume. Consequently, in the simulations we placed the plume en-

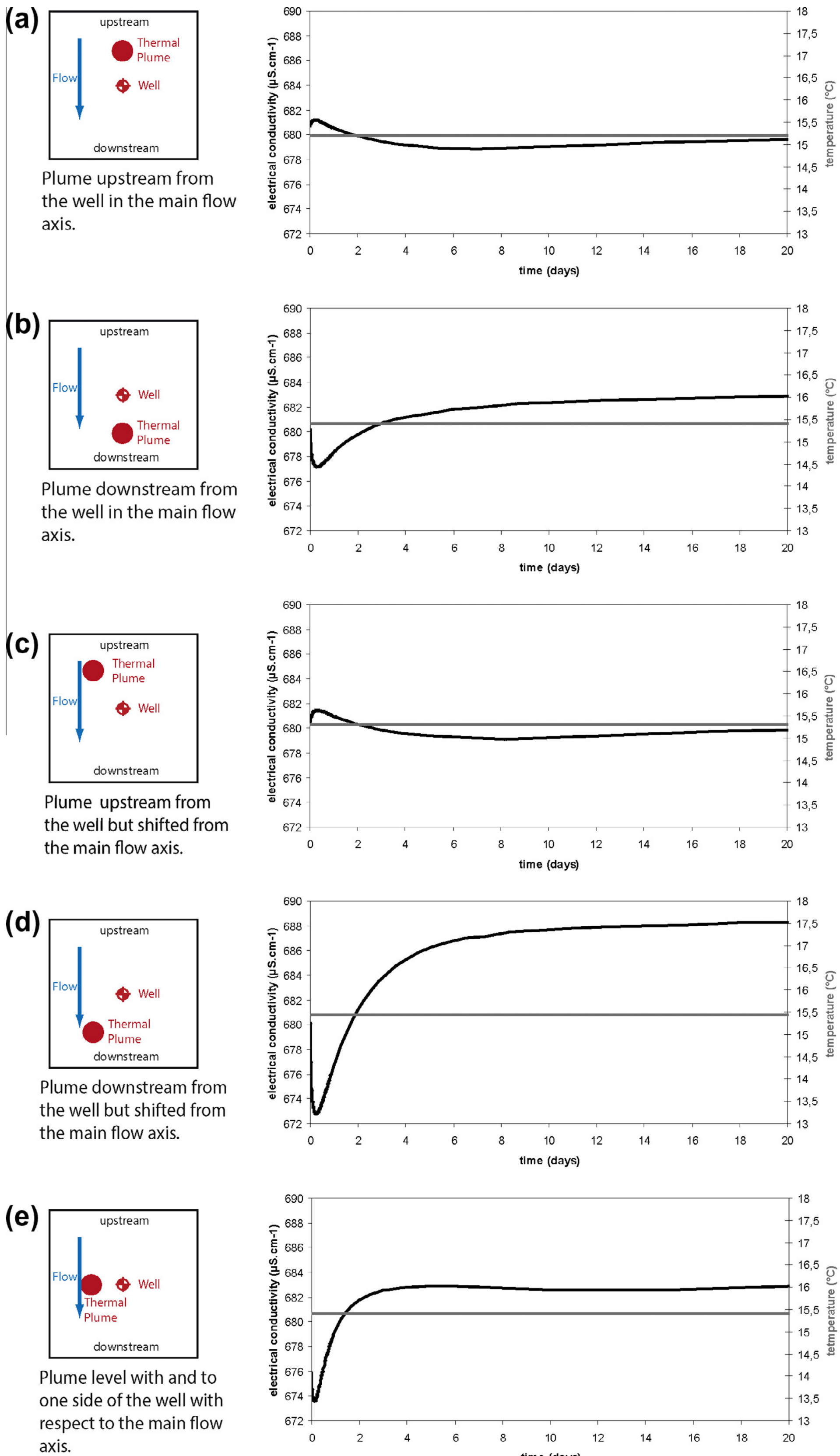

Fig. 6. Solute (equivalent to electrical conductivity) and thermal transport simulation for a single set of parameters as shown in Fig. 5 (hydraulic conductivities, storage coefficients, longitudinal and transversal dispersivities, etc.).

trance at the bottom of the Barremian, but we varied the position of the plume with respect to the well, which was fixed at the center of the simulated area. We tested five different plume-locations: directly upstream and downstream from the well with respect to the flow in the shallow aquifer; upstream and downstream but to one side of the well with respect to the flow direction; and level with and to one side of the well with respect to the flow in the shallow aquifer. We tested these different plume positions for a single set of hydrodynamic and hydrodispersive parameters (see Fig. 5a for hydrodynamic parameters and Fig. 6 for the plume positions tested). The average distance between the plume position and the well position was approximately 10 m, with this uncertainty being due to the distribution of the elements in the mesh.

The results (Fig. 6) shows that the upstream plume positions are incompatible with the graphs obtained during the real pumping test (both in solute transport and temperature transfer). Conversely, the downstream and level with the well plume positions allowed us to produce a decrease, followed by an increase in electrical conductivity, as in the measured data, even if no significant variations of temperature were simulated. This last point is discussed in the following part entitled "Transport behavior and boundary conditions". Despite there is not a perfectly match between the simulated temperature and the observed temperature, the downstream plume position is more consistent with the fact that the natural springs around Aix Marlioz, where the plume water and the subsurface aquifer water mix, are also downstream from the well. But this is not always the case, as further north there is evidence of another plume that rises 190-m upstream from the natural springs (Gallino, 2006).

5.2. Transport behavior and boundary conditions

Our simulations showed a negligible thermal effect (less than 0.1 °C), which led us to indicate a constant temperature in the results shown in Fig. 6. Although this does not correspond exactly to observed temperatures, which slowly increased from 15.5 to 17 °C, compared to the variation in electric conductivity, the amplitude of the temperature variations in our data was very small and this small amplitude was confirmed by the simulations. Given that the dispersivities applied to the simulations were the same for mass transport and thermal transport on one hand, and that the advective transport is given by a same set of velocities applied to mass and heat transport, this result needs to be explained. One possibility is that it is due to the difference between the solute transport diffusion that is mostly negligible and the heat transport diffusion that is not. Another possibility is that the boundary conditions resulted in quite homogenous temperatures at the bottom of the shallow aquifer. Indeed, the weakly mineralized water percolates through the whole upstream thickness of the aquifer, and we used this as a boundary condition for the upstream side of the model. The highly mineralized water is injected locally where the plume enters the bottom of the model. Because the final mineralization is obtained as the water passes through the thrust fault, the water already has its final mineralization when it enters the bottom of the plume in the model. Consequently, we used this as our boundary condition for the bottom of the model. The temperatures depend on the air temperature applied to the top of the shallow aquifer and to the heat flux from depth. Hence, if upstream water has the same mineralization or electrical conductivity as the water in the shallow aquifer, the upstream water will not have a homogenous temperature (there will be a thermal gradient with the lower part of the shallow aquifer being several degrees warmer than the surface temperature). In the case of a relatively slow upwelling that permits temperature exchanges with the surrounding rocks (greater at the Marlioz spa than in the Thermes Nationaux area, where the upwelling velocity and flow rate are greater), the temperature in the vicinity of the borehole will not be significantly different from the temperature of the shallow aquifer. This would explain the small amount of variation in both the observed and simulated temperature values.

A third explanation, which can be combined with the two previous ones, comes from the ratios in the mixing of the transport characteristics. A factor of two into the concentrations values between the two poles (thermal plume and shallow aquifer) exists whereas for the thermal characteristics a less marked contrast between these two poles is observed. When the mixing ratio is slightly imbalanced in favor of one of the two poles (thermal plume or shallow aquifer) the less marked contrast in temperature leads to a negligible thermal effect.

6. Conclusion

The present study produced two very interesting results:

(1) We were able to locate the plume at the bottom of the Barremian strata, with the only realistic position being downstream of the well. The plume cannot be upstream from the well.
(2) A pumping test on a single well can give enough information to substantially reduce the number of complementary investigations needed. In the present case, our results show that any additional drilling or geophysical prospecting should focus on the area downstream from the Ariana Well.

The advantage of this type of method is that it characterizes mixing zones on the basis of information from a single well, which is less expensive than integral pump-testing or hydraulic-tomography methods (Bauer et al., 2004; Li et al., 2007), which require several wells or piezometers.

Acknowledgements

The authors want to acknowledge Mrs I. Mercier-Bosseny, manager of Thermes de Marlioz Spa at the beginning of our project, for her interest to our research and who gave the authorization of monitoring all the outlets of Aix Marlioz. They are grateful to the Thermes de Marlioz Spa (Accor Group) and to the Rhône-Alpes region for their respective financial support. The authors wish to thank the unknown reviewers which helped us to improve the quality of the manuscript.

References

Bataillé, A., Genthon, P., Rabinowicz, M., Fritz, B., 2006. Modeling the coupling between free and forced convection in a vertical permeable slot: implications for the heat production of an enhanced geothermal system. Geothermics 35, 654–682.
Bauer, S., Bayer-Raich, M., Holder, T., Kolesar, C., Müller, D., Ptak, T., 2004. Quantification of groundwater contamination in an urban area using integral pumping tests. Journal of Contaminant Hydrol 75 (3–4), 183–213.
Bester, M.L., Frind, E.O., Molson, J.W., Rudolph, D.L., 2006. Numerical investigation of road salt impact on an urban wellfield. Ground Water 44 (2), 165–175.
Boberg, T.C., 1966. Calculation of the production rate of a thermally stimulated well. Journal of Petroleum Technology 18 (12), 1613–1623.
Boulton, N.S., 1954. Unsteady radial flow to a pumped well allowing for delayed yield from storage.
Cooper, H., Jacob, C., 1946. A generalized graphical method for evaluating formation constants and summarizing well field history. Transactions of the American Geophysical Union 27, 526–534.
Diersch, H.J.G., 1996. Interactive, Graphic-Based Finite Element Simulation System FEFLOW for Modeling Groundwater Flow, Contaminant Mass and Heat Transport Processes. Wasy, Berlin.
Gallino, S., Josnin, J.-Y., Dzikowski, M., Cornaton, F., Gasquet, D., 2009. The influence of paleoclimatic events on the functioning of an alpine thermal system (France): the contribution of hydrodynamic–thermal modelling. Hydrogeology Journal 17, 1887–1900.
Gallino, S., Dzikowski, M., Josnin, J.-Y., Gasquet, D., 2010. Characterization of the hydrogeological boundary separating two aquifers: a multi-disciplinary approach combining geological, geochemical and hydrodynamic data (Aix-les-Bains, France). Bulletin de la Societe Géologique de France 181 (4), 305–313.
Gallino, S., 2006. Le Karst du dôme anticlinal d'Aix-les-Bains: nouvelles données sur le panache hydrothermal. Karstologia 48, 29–32.
Gallino, S., 2007. Hydrogéologie, géochimie et modélisation hydrodynamique-thermique d'un système thermo-minéral associé un contact structural alpin (Aix-les-Bains - Savoie) [Hydrogeology, geochemistry and coupled

hydrodynamicthermical modeling of a thermo-mineral system associated with an alpine thrust (Aix-les-Bains, Savoie)]. PhD Thesis, Université de Savoie, France.
Grant, M.A., Bixley, P.F., Donaldson, I.G., 1983. Internal flows in geothermal wells: their identification and effect on the wellbore temperature and pressure profiles. SPE Journal 23 (1), 168–176.
Hamm, S.-Y., Bidaux, P., 1996. Dual-porosity fractal models for transient flow analysis in fissured rocks. Water Resources Research 32 (9), 2733–2745.
Hantush, M., 1956. Analysis of data from pumping tests in leaky aquifers. Transactions American Geophysical Union 37 (6), 702–714.
Holzbecher, E., 1998. Modeling density-driven flow in porous media. Principles, numerics, software. Springer, p. 287.
Jourde, H., Cornaton, F., Pistre, S., Bidaux, P., 2002. Flow behavior in a dual fracture network. Journal of Hydrology 266 (1–2), 99–119.
Kalbus, E., Schmidt, C., Bayer-Raich, M., Leschik, S., Reinstorf, F., Balcke, G.U., Schirmer, M., 2007. New methodology to investigate potential contaminant mass fluxes at the stream aquifer interface by combining integral pumping tests and streambed temperatures. Environmental Pollution 148, 808–816.
Keys, W.S., Brown, R.F., 1978. The use of temperature logs to trace the movement of injected water. Ground Water 16 (1), 32–48.
Leven, C., Dietrich, P., 2006. What information can we get from pumping tests?-comparing pumping test configurations using sensitivity coefficients? Journal of Hydrology 319 (1–4), 199–215.
Lucazeau, F., Vasseur, G., 1988. Heat density data from France and surrounding margins. Tectonophysics 164, 251–258.
Li, W., Englert, A., Cirpka, O.A., Vanderborght, J., Vereecken, H., 2007. Two-dimensional characterization of hydraulic heterogeneity by multiple pumping tests. Water Resources Research 43 (4), 1–13 (W04433).
Lods, G., Gouze, P., 2004. WTFM, software for well test analysis in fractured media combining fractionalflow with double porosity and leakance approaches. Computers and Geosciences 30, 937–947.
Miller, C., 1979. Wellbore storage effects in geothermal wells. Master degree, Lawrence Berkeley Laboratory, University of California, for the U.S. Department of Energy W-7405-ENG-48, 12p.
Özkahraman, H.T., Selver, R., Işik, E.C., 2004. Determination of the thermal conductivity rock from P-wave velocity. International Journal of Rock Mechanics and Mining Sciences 41 (4), 703–708.
Perrochet, P., Bérod, D., 1993. Stability of the standard Crank–Nicolson–Galerkin Scheme applied to the diffusion-convection equation: some new insights. Water Resources Research 29 (9), 3291–3297.
Pfingsten, W., Hadermann, J., Perrochet, P., 2001. Radionucleide release and transport from nuclear underground tests performed at Mururoa and Fangataufa: predictions under uncertainity. Journal of Contaminant Hydrology 47 (2–4), 349–363.
Renard, P., 2005a. The future of well hydraulics. Hydrogeology Journal 13 (1), 259–262.
Renard, P., 2005b. Hydraulics of Wells and Well Testing. In: Anderson, M.G. (Ed.), Encyclopedia of Hydrological Sciences. John Wiley and Sons, p. 3456.
Riva, M., Guadagnini, A., Bodin, J., Delay, F., 2009. Characterization of the hydrogeological experimental site of poitiers (France) by stochastic well testing analysis. Journal of Hydrology 369, 154–164. http://dx.doi.org/10.1016/j.jhydrol.2009.02.040.
Sagar, R., Doty, D.R., Schmidt, Z., 1991. Predicting temperature profiles in a flowing well. SPE Production Engineering 6 (4), 441–448.
Siméon, Y., 1980. Etude hydrogéologique des sources thermominérales de Tarentaise (Savoie): Brides-les-Bains, Salins-les-Thermes. Thèse, Université Scientifique et Médicale de Grenoble, La Léchère- Alpes Françaises, 219 p.
Sonney, R., 2010. Groundwater flow, heat and mass transport in geothermal systems of a Central Alpine Massif: the cases of Lavey-les-Bains, Saint Gervais-les-Bains and Val d'Illiez. PhD Thesis. University of Neuchâtel, Switzerland, 364 p.
Theis, C.V., 1935. The relation between the lowering of the piezometric surface and the rate and duration of discharge of a well using groundwater storage. Transactions of the American Geophysical Union 16, 519–524.
Thiébaud, E., Dzikowski, M., Gasquet, D., Renac, C., 2010. Reconstruction of groundwater flows and chemical water evolution in an amagmatic hydrothermal system (La Léchère, French Alps). Journal of Hydrology 381 (3–4), 189–202.
Vandebohede, A., Lebbe, L., 2006. Double forced gradient tracer test: performance and interpretation of a field test using a new solute transport model. Journal of Hydrology 317, 155–170.
Vuataz, F.-D., 1982. Hydrogéologie, géochimie et géothermie des eaux thermals de Suisse et des regions alpines limitrophes. Matériaux Pour la Géologie Suisse, Série Hydrologie 29, 174.
Waples, D.W., Waples, J.S., 2004. A review and evaluation of specific heat capacities of rocks, minerales and subsurface fluids, part 1: minerals and nonporous rocks. Natural Resources Research 13 (2), 97–122.
Warren, J.E., Root, P.J., 1963. The behaviour of naturally fractured reservoirs. Society of Petroleum Engineering Journal 3 (2), 245–255.
Woodbury, A.D., Smith, L., 1988. Simultaneous inversion of hydrogeologic and thermal data: 2. Incorporation of thermal data. Water Resources Research 24 (3), 356–372.